Published in final edited form as:
Biochim Biophys Acta. 2008 April ; 1778(4): 1120–1130. doi:10.1016/j.bbamem.2008.01.008.

CRAC motif peptide of the HIV-1 gp41 protein thins SOPC membranes and interacts with cholesterol

Alexander I. Greenwood[a], **Jianjun Pan**[a], **Thalia T. Mills**[a], **John F. Nagle**[a,b], **Richard M. Epand**[c], and **Stephanie Tristram-Nagle**[a,*]

a*Biological Physics Group, Physics Dept., Carnegie Mellon University, 5000 Forbes Avenue, Pittsburgh, PA 15213*

b*Dept. Biological Sciences, Carnegie Mellon University, 4000 Fifth Avenue, Pittsburgh, PA 15213*

c*Dept. Biochemistry/Biomedical Sciences, McMaster University, 1200 Main St. W., Hamilton, ON, Canada*

Abstract

This study uses low-angle (LAXS) and wide-angle (WAXS) x-ray synchrotron scattering, volume measurements and thin layer chromatography to determine structure and interactions of SOPC, SOPC/cholesterol mixtures, SOPC/peptide and SOPC/cholesterol/peptide mixtures. N-*acetyl*-LWYIK-amide (LWYIK) represents the naturally-occurring CRAC motif segment in the pretransmembrane region of the gp41 protein of HIV-1, and N-*acetyl*-IWYIK-amide (IWYIK), an unnatural isomer, is used as a control. Both peptides thin the SOPC bilayer by ~3 Å, and cause the area/unit cell (peptide+SOPC) to increase by ~9 $Å^2$ from the area/lipid of SOPC at 30 °C (67.0 ± 0.9 $Å^2$). Model fitting suggests that LWYIK's average position is slightly closer to the bilayer center than IWYIK's, and both peptides are just inside of the phosphate headgroup. Both peptides increase the wide-angle spacing d of SOPC without cholesterol, whereas with 50% cholesterol LWYIK increases d but IWYIK decreases d. TLC shows that LWYIK is more hydrophobic than IWYIK; this difference persists in peptide/SOPC 1:9 mole ratio mixtures. Both peptides counteract the chain ordering effect of cholesterol to roughly the same degree, and both decrease K_C, the bending modulus, thus increasing the SOPC membrane fluidity. Both peptides nucleate crystals of cholesterol, but the LWYIK-induced crystals are weaker and dissolve more easily.

Keywords

HIV-1; biomembranes; lipid bilayers; CRAC motif peptide; cholesterol crystals; SOPC

Introduction

Domain formation in membranes has generated considerable interest since the discovery of partitioning of cholesterol into detergent-insoluble lipid-specific fractions during cell membrane isolation [1]. These domains, or "rafts", are thought to sequester proteins that perform a specific role, such as GPI-anchored signaling via second messengers. In the HIV-1 membrane, there are two proteolytic cleaveage proteins of gp160 that may use lipid rafts: gp120, which recognizes and docks to the T-cell membrane, and gp41, which catalyzes the

*Corresponding author.

fusion step between the T-cell and the HIV membrane. A structural motif in the V3 loop of HIV-1 gp120 has a high affinity for both cholesterol and sphingomyelin [2]. In gp41 there is a highly-conserved consensus sequence having the pattern L/V-(X)(1-5)-Y-(X)(1-5)-R/K in which X(1-5) represents 1–5 residues of any amino acid. This sequence was first identified in the peripheral benzodiazapene receptor which may have a role in facilitating cholesterol transport into mitochondria [3]. This CRAC motif, or cholesterol recognition amino acid consensus sequence, is located adjacent to the transmembrane region of gp41. In HIV-1 this sequence is LWYIK, which has been shown to bind to cholesterol using cholesteryl-hemisuccinate agarose [4] and from studies using MAS/NMR and DSC [5]. HIV infection requires cholesterol in the HIV membrane [6] and mutations in the CRAC sequence reduce HIV infectivity [7].

In the present work, we use x-ray diffuse scattering to probe structure and material properties of SOPC membranes with the CRAC motif peptide LWYIK, or the non-CRAC motif isomer, IWYIK, in the absence and presence of cholesterol. These peptides are two of several with related sequences that were investigated by differential scanning calorimetry (DSC) [5,8], and differences were found in the abilities of these peptides to inhibit cholesterol/lipid interaction and to cause cholesterol crystallization. Addition of cholesterol to lipid membranes is well-known to progressively lower the enthalpy of the lipid's sharp main phase transition and to induce a broader melting component [9]. Addition of LWYIK, but not IWYIK, reversed this effect [8]. Both LWYIK and IWYIK caused crystals of cholesterol to form at a 9:1 SOPC/peptide mole ratio in 50 mole % SOPC/cholesterol mixtures, but the enthalpy of melting these crystals was almost two-fold higher in the IWYIK samples. This suggests that IWYIK binds to the SOPC thereby displacing cholesterol from its interaction with SOPC; cholesterol then crystallizes. By contrast, LWYIK may facilitate the segregation of cholesterol into cholesterol-rich domains by binding directly to cholesterol causing the sterol to surpass its solubility limit in the membrane.

Our recently developed low-angle x-ray diffuse scattering (LAXS) technique provides accurate structures of pure bilayers [10–13] and bilayer/cholesterol mixtures [14] in their fully hydrated, fluid (liquid-crystalline) state. This LAXS methodology provides the experimental form factors $F(q_z)$ of the bilayer, with and without peptide. These form factors are then fit to a model of the SOPC bilayer which provides structural information such as area and thickness of SOPC membranes with peptides. Diffuse LAXS data also provides the membrane bending modulus K_C that measures how much energy is required to bend the membrane ($E= ½ K_C C^2$, where the curvature $C=R^{-1}$, and R is the radius of curvature). In this study we determine how LWYIK and IWYIK affect K_C of SOPC membranes in the presence and absence of cholesterol. Wide-angle x-ray scattering (WAXS) enables us to determine how chain orientational order and lateral chain packing is affected by cholesterol and peptides [15,16]. In addition, the issue of precipitation of cholesterol crystals is examined using x-ray diffraction. Thin layer chromatography reveals the difference in hydrophobicity of these peptides. Finally, volume measurements are used in the SOPC bilayer structure determination [17].

Materials and Methods

Materials

1-stearoyl-2-oleoyl-*sn*-glycero-3-phosphocholine (SOPC) (Lot 180-181PC-48) was purchased from Avanti Polar Lipids (Alabaster, AL) in lyophilized form and used without further purification. D_2O/H_2O mixtures were made with Barnstead nanopure water and deuterium oxide (99.9 atom % D) (Aldrich, Milwaukee, WI). HPLC grade chloroform was purchased from Aldrich. The peptides N-*acetyl*-LWYIK-amide (LWYIK or L) and N-*acetyl*-IWYIK-amide (IWYIK or I) were purchased from the Biomedical Research Support Facilities, Synthetic Peptide Application Lab, at the University of Pittsburgh. Their purity was checked

at the Center for Molecular Analysis at Carnegie Mellon University using electrospray ionization mass spectrometry. Both were found to have the same molecular weight (763.4 Da) and a purity of >99%.

Thin layer chromatography (TLC)

TLC of lipids, peptides and peptide/lipid mixtures was carried out in order to discern any differences in the peptides, which had the same molecular weight, and also to determine if lipid and/or peptide breakdown occurred during x-ray exposure or during the experimental procedures. The protocol and results are described in Supplementary Material.

Volume measurements

Volume measurements of pure SOPC and SOPC/cholesterol mixtures were carried out as described in Greenwood et al., 2006 [18]. Mixtures of D_2O and H_2O were prepared at known densities. Chloroform was added to ~3 mg of dry SOPC or SOPC/cholesterol and then the solvent was evaporated using a stream of nitrogen and subsequent overnight drying in a fume hood. When peptides were used, they were first solubilized in methanol by vortexing and added to the lipids in chloroform before evaporation of solvent. 3 ml of the D_2O/H_2O mixture was added to the dried mixtures. The samples were hydrated by vortexing and thermal cycling three times between 50 °C and −20 °C. The samples were centrifuged at 1380xg in a Fisher Centrific 228 desktop centrifuge (Pittsburgh, PA) located within a home-built temperature controlled chamber which was maintained at 30 °C using a YSI Model 72 proportional temperature controller (Yellow Springs, OH). The lipid was observed to either sink or float, depending on its density relative to that of the D_2O/H_2O solution. Temperatures were accurate to ±0.5 °C and specific volumes were determined to an accuracy of ±0.0005 ml/g.

Light Scattering

The density centrifugation results for samples with peptides were difficult to read, often yielding both floating and sinking lipid in the same vial. Therefore, dynamic light scattering was carried out in order to determine the size of the multilamellar vesicles (MLVs) formed in the absence and presence of peptides and cholesterol. Dynamic light scattering (DLS) was carried out using a Malvern particle sizer (Worcestershire, UK) that was calibrated with a polystyrene bead standard of 8020 Å diameter. DLS measures Brownian motion and relates this to the size of the particles. 1.5 ml containing 0.5–1 mg MLVs, was loaded into a glass cuvette and the Brownian motion was monitored over 1 minute, nine times in succession and the results were averaged.

X-ray sample preparation and scattering experiments

4 mg SOPC or SOPC/cholesterol was first dissolved in chloroform, and peptide in a methanol stock solution was added in a 1:9 mole ratio to total lipid. The solvent was removed using a KNF filtration pump (Trenton, NJ). For oriented samples 200 μl 1:1 chloroform/methanol was added to this mixture which was then vortexed and plated onto 30x15x1 mm silicon wafers using the rock and roll technique [19,20]. Samples were dried one day in a glove box and one day in a fume hood and trimmed. Hydration from water vapor was then carried out in a thick-walled hydration chamber [11] and continued until the lamellar D-spacing was within 1–2 angstroms of the D-spacing obtained with excess water in x-ray capillaries (*vide infra*). Oriented x-ray data were taken at the Cornell High Energy Synchrotron Source (CHESS) using the G1 station on two separate trips with wavelength 1.2742 or 1.1797 +/− .012 Å. The beam was .2Hx.6Vmm or .2Hx.2V mm and the total beam intensity was 10^{11} photons/sec. The sample was ~10 micron thick along the normal to the ~2000 bilayers and its dimension along the direction of the beam was either narrow (5 mm) or wide (13 mm) for low-angle x-ray scattering (LAXS) on two separate trips, and narrow (4 mm) for wide-angle x-ray scattering

(WAXS) measurements. The flat samples were rotated from −3 to 7 degrees in θ relative to the beam during the 30–60 s LAXS exposure and were x-rayed at fixed θ for the 10–20 s WAXS exposure. For WAXS, θ = 0.2° was used to first collect lipid scattering and then θ = −0.2° was used to collect background chamber scattering that was subtracted from the lipid data. Data were collected using a Flicam CCD (Finger Lakes Instrumentation, Lima, NY) with a 1024 x 1024 pixel array and pixel size 0.06978 mm/pixel. The sample-to-CCD distance was 400 mm for LAXS and 155 mm for WAXS.

Fully hydrated D-spacings of samples in excess water were prepared by weighing 1 mg of dry sample thoroughly mixed (*vide supra*) with 40 μl milli-Q water into small nalgene vials. These were vortexed and thermally cycled three times between 50 °C and −20 °C and loaded into glass x-ray capillaries. These MLV samples were x-rayed at 30 °C using a Rigaku RUH3R microfocus rotating anode (Woodlands, TX) equipped with a Xenocs FOX2D focusing collimation optic. 5 minute scans were collected using a Rigaku Mercury CCD detector; silver behenate (D=58.367 Å) was used for calibration. Also, unilamellar vesicle (ULV) samples of pure SOPC were prepared by extrusion of MLVs through polycarbonate filters [11] and were x-rayed using the Rigaku RUH3R. Based on the binding experiments in Refs. 5 and 8, we estimate that ~97% of the peptide is bound to membranes in MLV and ULV samples.

Diffuse Low-Angle X-ray Scattering (LAXS) Data Analysis

The diffuse data analysis has been described previously in several publications [10–13,21] and will be reviewed here only briefly. The scattering intensity for a stack of oriented bilayers is the product: $I(\mathbf{q}) = S(\mathbf{q})|F(q_z)|^2/q_z$, where $\mathbf{q} = (q_r, q_z)$, $S(\mathbf{q})$ is the structure interference factor, $F(q_z)$ is the bilayer form factor and q_z^{-1} is the usual low-angle approximation to the Lorentz factor for narrow oriented samples for which all the sample remains in the beam for all relevant q. The Lorentz correction changes to q_z^{-2} for wide samples because the footprint of the beam on the sample is smaller than the sample for all relevant q. Diffuse x-ray scattering data that results from lipid samples near full hydration are analyzed using smectic liquid crystal theory [22]. In the first step, the theory is fit to the data to obtain two material parameters of bilayers: the bilayer bending modulus (K_C) and the compression modulus (B) and $|F(q_z)|^2/q_z$. In the second step, a structural analysis using the H2 model [17] determines the electron density with the Fourier transform that best fits the experimental $|F(q_z)|$. In the H2 model the headgroups (phosphate and carbonyl/glycerol) and the methyl trough are modeled as Gaussians, while the water/choline density and methylene regions are modeled as error functions [17]. Initially, the SOPC data were fit with only two constraints: D_{H1} = 4.95 Å (distance between average headgroup peak and the hydrocarbon region) and r = 1.9 (volume ratio of terminal methyl to methylene) [see 17]. For the IWYIK and LWYIK/SOPC samples the following parameters were fixed to be the same as those from the fit to the SOPC data: headgroup widths (2.54 Å (glycerol/carbonyl) and 2.62 Å (phosphate)), distance between the headgroups (3.78 Å), and widths of the error functions for the water/choline (2.96 Å) and the carbonyl densities (2.42 Å). An additional Gaussian was added for the peptide, and the position and width of the peptide were free parameters in the fit. Although a single Gaussian is a simplification of the peptide electron density distribution, this may be adequate to describe the peptide's average location in a fluctuating, fluid lipid bilayer. Structural analysis of samples with cholesterol will be deferred to a subsequent publication [14].

Wide-Angle X-ray Scattering (WAXS) Data Analysis

WAXS emanates primarily from chain scattering that is affected by interchain distances and chain orientational order. The orientational order is obtained from the angular dependence I (ϕ) (where $\tan \phi = q_z/q_r$) of WAXS data from oriented samples which are analyzed following [15,16,23,24]. The analysis assumes the Maier-Saupe distribution function [25],

$$f(\beta)=\frac{1}{Z}\exp(m\cos^2\beta) \quad (1)$$

where Z is a normalization factor that depends on m, β is the angle made with the bilayer normal, and the effective inverse width m is a fitting parameter. During fitting, a constant isotropic background is subtracted. An x-ray order parameter is then defined from the distribution in Eq. (1) as

$$S_{xray}=\frac{1}{2}\left(3\langle\cos^2\beta\rangle-1\right). \quad (2)$$

Results

Volumes

Fig. 1A shows the raw data for the apparent specific volumes v of mixtures of cholesterol with SOPC at 30 °C as a function of cholesterol mole fraction x. The main phase transition temperature of SOPC is 6 °C [26], so at 30 °C, SOPC is in the fluid, liquid-crystalline phase. Fig. 1B shows the volume per molecule V (lipid and cholesterol) in $Å^3$ as a function of x. The x=0 intercept is the partial molecular volume of lipid V_L and the intercept at x=1 is the partial molecular volume of cholesterol V_C [18]. The constant slope in Fig. 1B implies that V_L and V_C do not vary with x. Their values are V_L = 1311.3 $Å^3$ and V_C = 616 $Å^3$. This partial molecular volume of cholesterol is similar to that measured in mixtures with POPC, 623 $Å^3$ [18]. V_L = 1311.3 $Å^3$ is used in the H2 model for bilayer structure determination.

Light Scattering

Fig. 2A shows the size distribution of pure SOPC and SOPC/cholesterol MLVs (7:3 and 5:5 mole ratios) as prepared for the volume measurement. In all three cases there is primarily a single, average MLV size that is greater than 1 μm, which allows a clear visualization after density centrifugation. By contrast in Fig. 2B, in the presence of LWYIK there is at least a bimodal distribution of vesicles with a significant fraction at ~100 nm. This suggests that the peptide promotes the formation of smaller vesicles, which do not readily equilibrate during density centrifugation. These negative results led us to simply estimate the volume of the peptide to be 999 $Å^3$ based upon known volumes of amino acids [27].

X-Ray D-spacing results

Table 1 summarizes LAXS D-spacings obtained at 30 °C for SOPC with LWYIK and IWYIK in the presence of cholesterol at 30 and 50 mole % of total lipids. As shown, the low-angle lamellar D-spacing first increases at 30 mole % cholesterol, then decreases at higher mole fraction. In the absence of cholesterol, no D-spacing was measurable in the SOPC/peptide samples, since the MLVs unbound completely, i.e., the D-spacing went to infinity.

Table 1 also summarizes WAXS d-spacings which were essentially the same whether obtained from oriented samples (1:1 water:lipid) or from isotropic samples in capillaries in excess water (40:1 water:lipid). As shown, cholesterol causes an increase in d and the peptides do not significantly modify this increase in chain packing for 30 mole % cholesterol. However, at 50 mole % the two peptides have opposite effects on d; IWYIK causes a decrease (4.89 to 4.75 Å), while LWYIK causes an increase (4.89 to 5.01 Å). Although this is a small effect, it was observed reproducibly three times using both oriented and capillary samples.

Diffuse LAXS Results

Figure 3 shows the diffuse low-angle x-ray scattering from pure SOPC and SOPC/peptide samples. Fitting to the liquid crystal theory was carried out in the gray boxes as described in

Materials and Methods and the lobes are numbered as shown in Fig. 3A. As shown in Figs. 3B and C, both peptides increase the width of the diffuse lobes and weaken the third lobe. A separate mosaic spread experiment, which is a measure of the degree of misorientation of the lipid samples on the silicon substrates, obtained mosaic spreads of 0.05 °, 0.18 ° and 0.14 ° for the samples in Figs. 3A, B and C, respectively. This amount of mosaic spread has negligible effect on the fitting results to the liquid crystal theory, and is not the reason for changes in the diffuse patterns, but it does cause prominent arcs on the very intense h=1 and h=2 orders in the first lobe seen in Figs. 3B and 3 C.

The bending modulus, K_C, decreases when either peptide is added to the lipid and lipid/cholesterol samples as reported in Table 2. Table 2 also shows that addition of 30% cholesterol increases K_C for SOPC by a factor of 1.7. Both peptides reverse this effect of cholesterol, however, since the K_C values revert to those without cholesterol when either peptide is added in a 1:9 mole ratio to the SOPC/30 mole % cholesterol samples.

The fitting analysis obtains $|F(q_z)|$, which is shown in Fig. 4 for SOPC and SOPC/peptide (9:1). As shown there is a movement towards higher q_z of the positions of the zeroes (at q_z = 0.26 $Å^{-1}$ and 0.41 $Å^{-1}$) for both peptides relative to SOPC. A movement towards higher q_z suggests a thinning of the bilayer. The lack of data in the first lobe did not affect the structural comparison, as we concluded from analyzing the SOPC sample without ULV data. The F(0) point, shown at q_z = 0, was obtained using area and volume data as in [28].

The fits of the H2 model in q-space are shown in Fig. 4. Fig. 5A shows the corresponding electron density in real space with the contributions to the total electron density from the component groups of the lipid. In Fig. 5B the peptide Gaussian is also shown. The hydrocarbon thickness of the bilayer, 2Dc, is smaller than that of SOPC by 3 Å in the presence of each peptide. The area obtained from the H2 model for the unit cell (defined as one lipid plus x/(1-x) peptide) increases from that of SOPC by ~ 9 $Å^2$. When the starting position for the peptide was moved 5 Å inwards or outwards from that shown in Fig. 5B, the fitting program rapidly returned it to its position near 17 Å from the center of the bilayer, so this value appears to be robust. These structural results are summarized in Table 2.

Hydrocarbon thicknesses and area per unit cell were not obtained for the samples with both cholesterol and peptide because fitting data for a three-component system proved over-parameterized for reliable structure determination. However, even with inaccurate individual parameters, the head-head thickness D_{HH}, which is the distance between the two headgroup peaks in the electron density profile, tends to be a robust quantity, so its value is estimated in Table 2 when both cholesterol and peptides are added to SOPC.

WAXS Results

Figure 6 shows the WAXS intensity collected on a two-dimensional CCD. These data were obtained for oriented samples with a lamellar D-spacing ~10 Å less than full hydration, but subsequent full hydration to a D-spacing that matched that obtained from MLVs in excess water (40:1) did not change these patterns (see Table 1), except to add broad water scattering centered at q_r = 2.0 $Å^{-1}$ (data not shown). The patterns in Fig. 6B and C for SOPC/peptide appear somewhat more extended to larger ϕ than for SOPC in Fig. 6A. We quantify this qualitative observation using the WAXS analysis [23,24] that obtains the chain orientational order parameters S_{xray} shown in Table 2. The WAXS pattern appears less extended for SOPC/30 mole % cholesterol (Fig. 6D) and S_{xray} increases by a factor of two in Table 2. When the peptides are added to SOPC with 30% cholesterol, the ϕ extension increases in Figs. 6E and 6 F compared to 6 D and S_{xray} decreases to near its value for pure SOPC.

Crystalline cholesterol X-ray diffraction results at high cholesterol content

Figure 7 shows the x-ray diffraction patterns in the wide-angle region resulting from inclusion of either peptide with SOPC/50% cholesterol membranes. Either peptide induced the initial formation of oriented, 3D crystals during the rock and roll procedure which produced a highly crystalline oriented pattern as shown in Fig. 7A and B, as compared with a few unoriented crystalline reflections in the wide-angle pattern of dried SOPC/50% cholesterol membranes (Figure 7C). The crystalline pattern induced by IWYIK had stronger, sharper reflections in several samples than did the LWYIK patterns.

The intensities of the peaks in each of the columns of reflections were analyzed by integrating the intensity along slices in the q_z direction. Figure 8 shows representative q_z-values for columns 2 and 4 in Fig. 7A. For columns 1, 2 and 3, the D-spacings were twice (68 ± 2 Å) that of the length of the cholesterol crystal spacing [29] which in turn is about two times the length of a single cholesterol molecule (~17 Å). However, column 4 had Bragg orders that could only be fit to a D-spacing near 34.3 ± 0.2 Å as shown in Figure 8, typical of the D-spacing obtained from the cholesterol crystal structure [29]. Columns 5, 6 and 7 in Fig. 7A were more difficult to measure due to the curvature of the reflections. Indeed, in one sample with LWYIK, the crystalline pattern was completely isotropic with no vertical columns (data not shown). The measured D-spacings obtained from SOPC/I and SOPC/L shown in Fig. 7A and B were the same within our uncertainty; samples in Fig. 7A and B had a lamellar LAXS D-spacing of 55.5 ± 0.1 Å for q_r= 0 slice, while the lamellar repeat of the sample shown in Fig. 7C was 56.9 Å.

A radial average of cholesterol monohydrate had no Bragg reflections corresponding to distances between 7 and 11 Å [30], but in this work there are 4 columns of reflections in this region. Thus, these crystals are more similar to anhydrous cholesterol [31], but they are not identical to anhydrous cholesterol since a radial average of the pattern in Fig. 7A (not shown) was different from the radial average of anhydrous cholesterol in Fig. 3A in Ref. 31. In our hands these crystals disappeared with humidity, rather than slowly converting to cholesterol monohydrate in water as does anhydrous cholesterol [31], although there may have been very small crystallites of cholesterol monohydrate that were undetectable by our methods.

It was of interest to compare the stability of these 3D crystals induced by each peptide in SOPC/50% cholesterol mixtures. In general, the crystals formed with LWYIK were less stable than those formed in the presence of IWYIK. When heated to 50 °C and annealed at high humidity for two hours, the patterns of both types of crystals started to fade as determined by subsequent x-ray diffraction at 45 °C, but more so in the LWYIK sample. Both types of crystals eventually disappeared over the course of several days in a high humidity environment at 30 °C.

In several samples prepared at 50% cholesterol with either peptide, there were no crystals at all, suggesting that crystallization may depend on the sample preparation as Huang et al. observed in some mixtures of PCs and PEs near 50% cholesterol [30]. These samples are close to the solubility limit of cholesterol, determined in dry POPC [30], and the peptides nucleate the crystallization.

Discussion

The CRAC motif's main role, reportedly, is to recognize cholesterol [3,4]. This study examines the effects of LWYIK on the physical properties of SOPC or SOPC/cholesterol membranes and compares to the effects of the non-CRAC motif isomer, IWYIK. The choice of SOPC as the lipid membrane was to compare to the previous DSC investigations [5,8]. The physical properties of SOPC, such as structure, volume, interactions and stiffness, have not previously been studied in our laboratory, so it was necessary to perform a thorough study of this control lipid in order to quantify the effects of the peptides. This discussion section begins with the

SOPC and SOPC/cholesterol control systems, which are of interest in their own right, and ends with the effects of LWYIK and IWYIK, and their implications for raft formation.

Lipid Bilayer Controls

The first important result from this work is the structure of fully hydrated SOPC, obtained as described above using the LAXS diffuse scattering method. In order to obtain this structure, the molecular volume V_L is first obtained using density centrifugation as described above. At 30°C, V_L = 1311.3 Å^3 for fully hydrated SOPC which agrees very well with the value 1311.2 Å^3 recently reported by Koenig and Gawrisch [32]. The difference between V_L for SOPC and DOPC (1302.3 Å^3) [18] is consistent with the difference in volumes of the two methylenes in SOPC that are replaced by HC=CH in DOPC, and the difference with V_L of POPC (1256.5 Å^3) [18] corresponds to the volumes of the extra two methylenes in SOPC [32].

Our area of 67.0 ± 0.9 Å^2 for SOPC is considerably larger than the value of 61.4 ± 0.6 Å^2 reported by Koenig et al., which they obtained using the modified gravimetric method [33]. Usually, the gravimetric method gives larger areas than ours, so this difference is unresolved. Our area is closer to POPC (68 ± 1.5 Å^2) [12] than to DOPC (72.4 ± 0.5 Å^2) [12]. A comparison of the areas of lipids with different amounts of unsaturation obtained from this laboratory using the same methodology is shown in Fig. 9. The trend of decreasing area with increasing chain length is confirmed in the mono-unsaturated lipids, as we have observed previously for di-saturated and di-unsaturated PC lipid areas. As shown in Fig. 9, addition of the first unsaturated bond on the *sn*-2 chain increases the area more than subsequent addition of an unsaturated bond on the *sn*-1 chain. The hydrocarbon bilayer thickness $2D_C$ (29.2 Å) reported in Table 3 is larger than that of POPC (27.1 Å) due to the longer stearoyl chain.

The S_{xray}, or chain orientational order parameter, was determined by the analysis of wide-angle scattering from oriented samples. Although S_{xray} and the NMR orientational order parameter that is often written as S_{NMR} measure different quantities, they both report similar qualitative trends [23]. S_{xray} ranges from 0.27 for DOPC at 25 °C to 0.44 for DPPC at 45 °C [24]. Even taking into account the temperature differences, our value of S_{xray} = 0.33 ± 0.03 for SOPC at 30 °C is intermediate between the values for the family of fully saturated DPPC and the family of di-unsaturated DOPC, and it is relatively closer in value to DOPC; this pattern for S_{xray} is similar to the pattern for area in Fig. 9.

Our value of the bending modulus K_C in Table 2 is in excellent agreement with that of 9.0 ± 0.6 x10^{-13} ergs obtained by Rawicz et al. [34] at 18 °C using the entirely different aspiration pipette technique. K_C for SOPC is close to that of POPC (8.5± 0.5 x10^{-13} ergs) [12] and DOPC (8.3 ± 0.2 x10^{-13}ergs) [10] (all at 30 °C). As emphasized by Rawicz et al. [34], K_C correlates very well with the square of hydrocarbon thickness $(2D_C)^2$. Another way to look at the comparisons between different lipids is in a plot similar to Fig. 9 but with K_C instead of A. Because K_C has a strong A dependence via D_C=V_C/A, this plot (not shown) is qualitatively similar to Fig. 9; indeed, SOPC and POPC are intermediate between the fully saturated and the diunsaturated families of lipids, but the volume of the hydrocarbon region V_C also plays a role. Our second set of control samples for the effect of CRAC motif peptides is SOPC with varying amounts of cholesterol. The structure of lipid bilayers with cholesterol is a major research project in our laboratory and structural values are not yet finalized. However, the following results suffice for the present study.

The partial molecular volume of SOPC does not change as cholesterol is added to SOPC up to 50 mole %, as indicated by Fig. 1B. This behavior is similar to DOPC and POPC, but it is unlike DMPC (all at 30 °C), sphingomyelin (at 45 °C) and DPPC (at 50 °C), which show a change in slope due to a volume condensation (at 20–30 mole %) caused by cholesterol [18] that could be due to lateral phase separation. Our SOPC result suggests that there is no phase

separation at 30 °C, consistent with T being sufficiently greater than the chain melting T_M = 6 °C for SOPC [26]. This is also consistent with our analysis of our WAXS data. When there is phase coexistence, the fit of the I(ϕ) intensity usually requires two of the distributions in Eq. 1, each with a different value of S_{xray} [23], but only one distribution is required to fit our SOPC/cholesterol data.

As also shown in Table 2, the addition of 30 mole % cholesterol causes S_{xray} to double and the bilayer also becomes thicker, as indicated by the head-head thickness D_{HH}, which can be robustly obtained even without determining hydrocarbon thickness $2D_C$. In other lipid/cholesterol systems, the trend in S_{xray} follows the trend in order parameter, S_{NMR} [23]. Upon addition of 30% cholesterol, the bilayer stiffens as shown by the 50% increase of the bending modulus K_C. Similar changes in both K_C and S_{NMR} were also observed in the case of POPC and cholesterol [35].

When cholesterol is added to SOPC, the fully hydrated LAXS D-spacing is observed to first increase at 30% and then decrease at 50% (Table 1). This trend is similar to what has been observed for other lipids [36,37]. The WAXS data (Table 1) show that cholesterol increases d, as was also observed by Finean for SOPC/cholesterol mixtures [38] and by Maulik and Shipley for N-stearoylsphingomylein [39]. This does not imply that the area/lipid increases with added cholesterol because the WAXS d-spacing is only one of two major factors related to the area/lipid. The other factor decreases as the orientational order parameter S_{xray} increases with cholesterol, so even though the wide angle d-spacing increases, the area/lipid decreases [24]. However, the area/unit cell (lipid plus cholesterol) does increase as shown in Table 2.

Effect of Peptides

Table 2 reports that when IWYIK or LWYIK is added to SOPC membranes, the bilayer thickness ($2D_C$ and D_{HH}) decreases by 3 Å for both peptides. When the peptides are added to SOPC with 30% cholesterol, D_{HH} decreases by 2 Å, a little less than when there is no cholesterol. The position of the peptides is between the phosphates and the glycerol groups of the lipids, but nearer to the phosphates. LWYIK, which is more hydrophobic according to TLC, resides slightly closer to the center of the bilayer by ~0.3 Å. The unit cell area A (consisting of one lipid plus x/(1-x) cholesterol), was the same for both peptides, 75.8 $Å^2$ for LWYIK/SOPC vs. 75.7 $Å^2$ for IWYIK/SOPC (1:9). Our result that LWYIK's position is 17.0 Å from the bilayer center is different from an energy minimization calculation which places LWYIK inside of the glycerol-carbonyl region [8], although that was for a DPPC bilayer rather than a SOPC bilayer. We note that the peptide has an average value for its depth of insertion into membranes, but not all amino acids in the peptide need have the same location. For example, the charged NH_3^+ of the Lys is likely to be in water, while the indole ring of the Trp is large and may extend more deeply into the bilayer.

The order parameter S_{xray} measured from oriented WAXS data (Table 2) also decreased by a factor of ~2/3 when either peptide was added to SOPC. Thus, the LAXS and WAXS results are consistent, because thickening of a bilayer is well-known to be correlated with chains that have larger orientational order parameters. Of course, whether a particular peptide increases or decreases thickness and order parameter depends upon how the peptide interacts with the particular membrane. It does seem plausible that a short peptide containing only 5 amino acids that stays near the bilayer surface would increase the area of each lipid headgroup in the interfacial region where the headgroup would have to share the volume with the added peptide. This would force the hydrocarbon chains of the lipid to also assume the same larger unit cell area, and it would require the hydrocarbon region to become thinner because there is little change in chain volume. This would then require a shorter average chain extension along the bilayer normal, which, in turn, would require more gauche rotations and a smaller orientational order parameter S_{xray}.

The results of this study are qualitatively similar to other x-ray studies of longer peptides. Hristova et al. [40] found that an 18 residue amphipathic helix (18A) with a volume concentration of peptide 1.4 times as large as our study resided at the bilayer interface and caused DOPC membrane thinning of ~2.6 Å. Thus the extent of thinning was smaller in [40], but the water content was also much smaller, 5.7 waters/lipid, compared to 29.7 waters/lipid in our study, which may cause crowding of headgroups in multibilayer sheets. The position of the 18A peptide was close to the glycerol region, not to the phosphate as in this study. In another investigation, Chen et al. [41] found a thinning of 2.0 Å when the 20-residue hydrophobic peptide alamethicin (Alm) was added to diphytanoylPC membranes with a volume concentration of peptide 0.9 times as large as our study. At their concentration (4 mole %), Alm was shown to be fully inserted across the membrane using oriented CD [41].

Several NMR studies have shown varying effects of peptides on the NMR chain order parameter S_{NMR} [42,43]. In POPC membranes with ~5 mole % of a transmembrane synthetic peptide of varying length, the change in the order parameter S_{NMR} was related to the hydrophobic mismatch: the peptide shorter than the bilayer width decreased the order parameter, while the peptide longer than the bilayer width increased it [44]. These changes are consistent with the hypothesis that a decrease of S_{NMR} induced by a peptide correlates with a thinner membrane.

As is also shown in Table 2, a similar decrease in S_{xray} by a factor of ~2/3 is caused by the addition of either peptide to SOPC with 30% cholesterol as well as without cholesterol. This nearly reverses the ordering effect caused by cholesterol. Another indication that the LWYIK and IWYIK peptides increase the fluidity of membranes is provided by our observed decreases in the bending modulus K_C in Table 2. Remarkably, these peptides reduce K_C to essentially the same values in SOPC bilayers both with and without 30% cholesterol, even though cholesterol itself increases K_C of SOPC. Our result that IWYIK reduces K_C by twice as much as LWYIK whereas both peptides reduce S_{xray} by the same amount indicates that K_C and S_{xray} are different measures of membrane fluidity.

In the case of the fusion peptide FP-23 of HIV, the even larger decrease in K_C reduces the energy required to form curved intermediates necessary for fusion, thereby facilitating the viral fusion process [45]. A change in stiffness may not be the primary role of the CRAC motif in the viral membrane because Table 2 shows that the control IWYIK reduces K_C almost twice as much as the CRAC peptide LWYIK. However, recent AFM studies have shown that immature HIV virions are 14-fold stiffer than mature virions [46], suggesting that the softening effect of LWYIK may aid in viral infection.

When IWYIK or LWYIK is added to SOPC membranes in a 1:9 mole ratio, the oriented samples take up much more water than SOPC alone (Table 1). In MLV experiments in excess water, either peptide causes complete unbinding; i.e., the distance between the bilayers increases such that the lamellar periodicity is lost. Two causes of this behavior are (1) charge repulsion due to the positively charged lysine amino acid on each peptide and (2) an increased fluctuation repulsive interaction between bilayers that follows from the smaller K_C values shown in Table 2 [47]. This is qualitatively similar to the case of the positively charged fusion peptide (FP23) of HIV-1 [45]. However, when 30 or 50 mole % cholesterol is added to the SOPC/peptide mixtures, the MLVs remain bound (Table 1). This somewhat surprising result can not be explained by a smaller repulsive fluctuation interaction, because the K_C value at 30% cholesterol in the presence of either peptide is nearly the same as without cholesterol (Table 2). It also does not seem likely that the charged state of the peptides is different with and without membranes as the experiments were performed near neutral pH and the pK of the lysine is near 10. pH measurements revealed only a slight acidification caused by cholesterol that was little changed with the addition of peptides. For these fully hydrated lipids, the

hydration repulsive interaction [48] is rather small. We suggest that there is an increase in the van der Waals attraction between neighboring bilayers in the presence of cholesterol that is strong enough to keep them from unbinding. An increase in the van der Waals attractive force between bilayers was predicted from egg PC/cholesterol data [49].

Table 1 shows that a small increase (~.06 Å) in the in-plane WAXS d-spacing occurs when either peptide is added to SOPC, but that no increase occurs when either peptide is added to SOPC with 30% cholesterol. Extrapolating this trend to 50% cholesterol would predict that d would decrease upon peptide addition, as it does for IWYIK, unless the association of the peptide undergoes an essential shift. The observed increase in d for LWYIK with 50% cholesterol suggests that LWYIK may shift from a surface state to an inserted state. This is consistent with the hypothesis that the CRAC motif makes a difference when the cholesterol concentration is high enough. Preferential positioning of LWYIK adjacent to cholesterol may be critical for nucleation of the raft domain needed for fusion of the HIV and host cell membranes. This also supports the MAS/NMR result that insertion of LWYIK into the membrane is promoted by the presence of cholesterol [5].

Since the wide-angle x-ray data could be fit by a single distribution (Eq. 1) [50], these peptides do not appear to induce domain formation, or liquid-liquid phase coexistence, in SOPC/30% cholesterol/peptide mixtures, although they may produce small size clusters of molecules and non-ideal mixing. However, at 50% cholesterol there was extensive crystallization of cholesterol in some of our oriented samples that is a dramatic form of phase separation. This result is similar to that observed using DSC; in suspension with excess buffer, LWYIK was shown to promote cholesterol crystal formation even at 40% cholesterol [5] and IWYIK also promoted cholesterol crystal formation at this lower cholesterol mol fraction [8], well removed from the solubility limit of cholesterol in PC. The anhydrous crystals of cholesterol that were formed were stable to several DSC heating and cooling cycles [5,8].

Although it is not immediately obvious what LWYIK/cholesterol interactions could accomplish both binding to cholesterol [4] and restoring the main chain melting transition in SOPC/cholesterol membranes [8], it may be that LWYIK sequesters cholesterol by binding to multiple cholesterol molecules and allowing them to crystallize around it. These cholesterol crystals would have LWYIK intercalated into them, which would reduce the anhydrous cholesterol melting peak [8] and x-ray diffraction Bragg orders relative to the control peptide, IWYIK, as observed in this paper. The weak and unstable crystalline patterns we obtained in the LWYIK/SOPC mixtures support this idea. Because IWYIK produces the strongest cholesterol crystals but a less significant increase in the chain melting peak [8], it could be surmised that this peptide does not intercalate into the cholesterol crystals but instead induces them by disrupting the lipid/cholesterol packing. This would then increase the local concentration of cholesterol and allow it to crystallize into the well-defined pattern in the IWYIK/SOPC mixtures that we observed. Since mutations in the CRAC motif [7] and depletion of cholesterol [6] each inhibit HIV infection, specific LWYIK-cholesterol domain formation may be required for membrane fusion. The HIV membrane has an unusually high cholesterol content [51,52], which suggests domain formation *in vivo* may include cholesterol crystallization.

Supplementary Material

Refer to Web version on PubMed Central for supplementary material.

Acknowledgements

This research was funded by grant GM 44976 from the General Medicine Institute of the US National Institutes of Health. Synchrotron beam time was provided by the Cornell High Energy Synchrotron Source which is funded by US

National Science Foundation grant DMR-0225180. We also acknowledge support from the Canadian Institutes of Health Research (grant 85008) (RME).The data for this study were taken on two visits to the G1 station and we thank Dr. Arthur Woll for his help in setting up, and D. Dipon Ghosh for help in collecting data at CHESS. The authors would also like to thank Dr. Raquel Epand for helpful discussions, Jordan Bates for help with experiments at CMU and Dr. Norbert Kuèerka for adding a third Gaussian for the peptide to the H2 model.

References

1. Brown DA, London E. Structure and Origin of Ordered Lipid Domains in Biological Membranes. J Membrane Biol 1990;164:103–114. [PubMed: 9662555]
2. Mahfoud M, Mylvaganam R, Lingwood CA, Fantini J. A novel soluble analog of the HIV-1 fusion cofactor, globotriaosylceramide (GB(3)), eliminates the cholesterol requirement for high affinity gp120/Bg(3) interaction. J Lipid Research 2002;43:1670–1679. [PubMed: 12364551]
3. Li H, Papadopoulos V. Peripheral-type benzodiazepine receptor function in cholesterol transport. Identification of a putative cholesterol recognition/interaction amino acid sequence and consensus pattern. Endocrinology 1998;139:4991–4997. [PubMed: 9832438]
4. Vincent N, Genin C, Malvoisin E. Identification of a conserved domain of the HIV-1 transmembrane protein gp41 which interacts with cholesteryl groups. Biochim Biophys Acta 2002;1567:157–164. [PubMed: 12488049]
5. Epand RM, Sayer BG, Epand RF. Peptide-induced formation of cholesterol-rich domains. Biochemistry 2003;42:14677–14689. [PubMed: 14661981]
6. Liao ZH, Graham DR, Hildreth JFK. Lipid rafts and HIV pathogenesis: Virion-associated cholesterol is required for fusion and infection of susceptible cells. AIDS Res Human Retroviruses 2003;19:675–687. [PubMed: 13678470]
7. Salzwedel K, West JT, Hunter E. A conserved tryptophan-rich motif in the membrane-proximal region of the human immunodeficiency virus type 1 gp41 ectodomain is important for Env-mediated fusion and virus infectivity. J Virol 1999;73:2469–2480. [PubMed: 9971832]
8. Epand RF, Thomas A, Brasseur R, Vishwanathan SA, Hunter E, Epand RM. Juxtamembrane protein segments that contribute to recruitment of cholesterol into domains. Biochemistry 2006;45:6105–6114. [PubMed: 16681383]
9. Mabrey S, Mateo PL, Sturtevant JM. High-sensitivity scanning calorimetric study of mixtures of cholesterol with dimyristoyl- and dipalmitoylphosphatidylcholines. Biochemistry 1978;17:2464–2468. [PubMed: 581060]
10. Liu Y, Nagle JF. Diffuse scattering provides material parameters and electron density profiles of biomembranes. Phys Rev E 2004;69:040901, 1–4.
11. Kuerka N, Liu Y, Chu N, Petrache HI, Tristram-Nagle S, Nagle JF. Structure of fully hydrated fluid phase DMPC and DLPC lipid bilayers using X-ray scattering from oriented multilamellar arrays and from unilamellar vesicles. Biophys J 2005;88:1–12. [PubMed: 15501938]
12. Kuerka N, Tristram-Nagle S, Nagle JF. Structure of fully hydrated fluid phase lipid bilayers with monounsaturated chains. J Memb Biol 2005;208:193–202.
13. Kuerka N, Tristram-Nagle S, Nagle JF. Closer look at structure of fully hydrated fluid phase DPPC bilayers. Biophys J: Biophys Letts 2006:L83–L85.
14. Pan JJ, Tristram-Nagle S, Mills TT, Nagle JF. Cholesterol modification of structure, interactions, and elasticity of lipid membranes depends on chain unsaturation. Phys Rev E. 2008(in preparation)
15. Levine, YK. Ph. D. Thesis. University of London; 1970. X-ray diffraction studies of oriented biomolecular layers of phospholipids.
16. Leadbetter AJ, Norris EK. Distribution functions in three liquid crystals from x-ray diffraction measurements. Mol Phys 1979;38:669–686.
17. Klauda JB, Kuerka N, Brooks BR, Pastor RW, Nagle JF. Simulation-based methods for interpreting X-ray data from lipid bilayers. Biophys J 2006;90:2796–2807. [PubMed: 16443652]
18. Greenwood AI, Tristram-Nagle S, Nagle JF. Partial molecular volumes of lipid and cholesterol. Chem Phys Lipids 2006;143:1–10. [PubMed: 16737691]
19. Tristram-Nagle S, Suter RM, Worthington CR, Sun WJ, Nagle JF. Measurement of chain tilt angle in fully hydrated bilayers of gel phase lecithins. Biophys J 1993;69:2558–2562.

20. Tristram-Nagle, S. Preparation of oriented, fully hydrated lipid samples for structure determination using x-ray scattering. Methods in Molecular Biology. In: Dopico, AM., editor. Methods in Membrane Lipids. 400. Humana Press; Totowa, NJ: 2007. p. 63-75.
21. Lyatskaya Y, Liu Y, Tristram-Nagle S, Katsaras J, Nagle JF. Method for obtaining structure and interactions from oriented lipid bilayers. Phys Rev E 2001;63:0119071–0119079.
22. DeGennes, PG.; Prost, J. The Physics of Liquid Crystals. Oxford Univ. Press; N.Y.: 1995.
23. Mills, TT. Ph.D. Thesis. Cornell University; 2007. Wide-angle X-ray scattering probes chain order and identifies liquid-liquid phase coexistence in oriented lipid membranes.
24. Mills TT, Toombes GES, Tristram-Nagle S, Smilgies DM, Feigenson GW, Nagle JF. Order parameters and areas in fluid-phase oriented lipid membranes using wide-angle x-ray scattering. Biophys J. 2007(submitted)
25. Maier VW, Saupe A. Eine einfache molekulare Theorie des nematischen kristallinflussigen Zustandes. Z Naturforsch 1958;13:564–566.
26. Vilcheze C, McMullen TPW, McElhaney RN, Bittman R. The effect of side-chain analogues of cholesterol on the thermotropic phase behavior of 1-steroyl-2-oleoylphosphatidylcholine bilayers: a differential scanning calorimetric study. Biochim Biophys Acta 1996;1279:235–242. [PubMed: 8603092]
27. Cohn, EJ.; Edsall, JT. Proteins, amino acids and peptides as ions and dipolar ions, Reinhold Publishing Corporation. New York: 1943. p. 155-176.p. 370-381.
28. Nagle JF, Wiener MC. Relations for lipid bilayers: connection of electron density profiles to other structural quantities. Biophys J 1989;55:309–313. [PubMed: 2713444]
29. Shieh HS, Hoard LG, Nordman CE. Crystal structure of anhydrous cholesterol. Nature 1977;267:287–289. [PubMed: 865625]
30. Huang J, Buboltz JT, Feigenson GW. Maximum solubility of cholesterol in phosphatidylcholine and phosphatidylethanolamine bilayers. Biochim Biophys Acta 1999;1417:89–100. [PubMed: 10076038]
31. Loomis CR, Shipley GG, Small DM. The phase behavior of hydrated cholesterol. J Lipid Research 1979;20:525–535. [PubMed: 458269]
32. Koenig BW, Gawrisch K. Specific volumes of unsaturated phosphatidylcholines in the liquid crystalline lamellar phase. Biochim Biophys Acta 2005;1715:65–70. [PubMed: 16109383]
33. Koenig BW, Strey HH, Gawrisch K. Membrane lateral compressibility determined by NMR and X-ray diffraction: Effect of acyl chain polyunsaturation. Biophys J 1997;73:1954–1966. [PubMed: 9336191]
34. Rawicz W, Olbrich KC, McIntosh T, Needham D, Evans E. Effect of chain length and unsaturation on elasticity of lipid bilayers. Biophys J 2000;79:328–339. [PubMed: 10866959]
35. Henriksen J, Rowat AC, Brief E, Hsueh YW, Thewalt JL, Zuckermann MJ, Ipsen JH. Universal behavior of membranes with sterols. Biophys J 2006;90:1639–1649. [PubMed: 16326903]
36. Petrache H, Harries D, Parsegian VA. Alteration of lipid membrane rigidity by cholesterol and its metabolic precursors. Macromol Symp 2005;219:39–50.
37. Ladbrook BD, Williams RM, Chapman D. Studies on lecithin-cholesterol-water interactions by differential scanning calorimetry and x-ray diffraction. Biochim Biophys Acta 1968;150:333–340. [PubMed: 5689845]
38. Finean JB. Interaction between cholesterol and phospholipids in hydrated bilayers. Chem Phys Lipids 1990;54:147–156.
39. Maulik PR, Shipley GG. Interactions of N-stearoyl sphingomyelin with cholesterol and dipalmitoylphosphatidylcholine in bilayer membranes. Biophys J 1996;70:2256–2265. [PubMed: 9172749]
40. Hristova K, Wimley WC, Mishra VK, Anantharamiah GM, Segrest JP, White SH. An Amphipathic α-helix at a membrane interface: a structural study using a novel x-ray diffraction method. J Mol Biol 1999;290:99–117. [PubMed: 10388560]
41. Chen FU, Lee MT, Huang HW. Evidence for membrane thinning effect as the mechanism for peptide-induced pore formation. Biophys J 2003;84:3751–3758. [PubMed: 12770881]

42. Henzler-Wildman KA, Martinez GV, Brown MF, Ramamoorthy A. Perturbation of the hydrophobic core of lipid bilayers by the human antimicrobial peptide LL-37. Biochemistry 2004;43:8459–8469. [PubMed: 15222757]
43. Dave PC, Tiburu EK, Damodaran K, Lorigan GA. Investigating structural changes in the lipid bilayer upon insertion of the transmembrane domain of the membrane-bound protein phospholamban utilizing ^{31}P and ^{2}H solid-state NMR spectroscopy. Biophys J 2004;86:1564–1573. [PubMed: 14990483]
44. Nezil FA, Bloom M. Combined influence of cholesterol and synthetic amphiphilic peptides upon bilayer thickness in model membranes. Biophys J 1992;61:1176–1183. [PubMed: 1600079]
45. Tristram-Nagle S, Nagle JF. HIV-1 fusion peptide decreases bending energy and promotes curved fusion intermediates. Biophys J 2007;93:2048–2055. [PubMed: 17526585]
46. Kol N, Shi Y, Tsvitov M, Barlam MD, Shneck RZ, Kay MS, Rousso I. A stiffness switch in human immunodeficiency virus. Biophys J 2007;92:1777–1783. [PubMed: 17158573]
47. Helfrich W. Steric interaction of fluid membranes in multilayer systems. Z Naturforsch A 1978;33:305–315.
48. Rand RP, Parsegian VA. Hydration forces between phospholipids bilayers. Biochim Biophys Acta 1989;988:351–376.
49. McIntosh TJ, Magid AD, Simon SA. Cholesterol modifies the short-range repulsive interactions between phosphatidylcholine membranes. Biochemistry 1989;28:17–25. [PubMed: 2706242]
50. Mills TT, Tristram-Nagle S, Heberle FA, Morales NF, Zhao J, Wu J, Toombes GES, Nagle JF, Feigenson GW. Liquid-liquid domains in bilayers detected by wide angle x-ray scattering. Biophys J. 2007(submitted)
51. Aloia RC, Tian HR, Jensen FC. Lipid-composition and fluidity of the human-immunodeficiency-virus envelope and host-cell plasma-membranes. Proc Natl Acad Sci USA 1993;90:5181–5185. [PubMed: 8389472]
52. Brugger B, Glass B, Haberkant P, Leibrecht I, Wieland FT, Krasslich HG. The HIV lipidome: A raft with an unusual composition. Proc Natl Acad Sci USA 2006;103:2641–2646. [PubMed: 16481622]

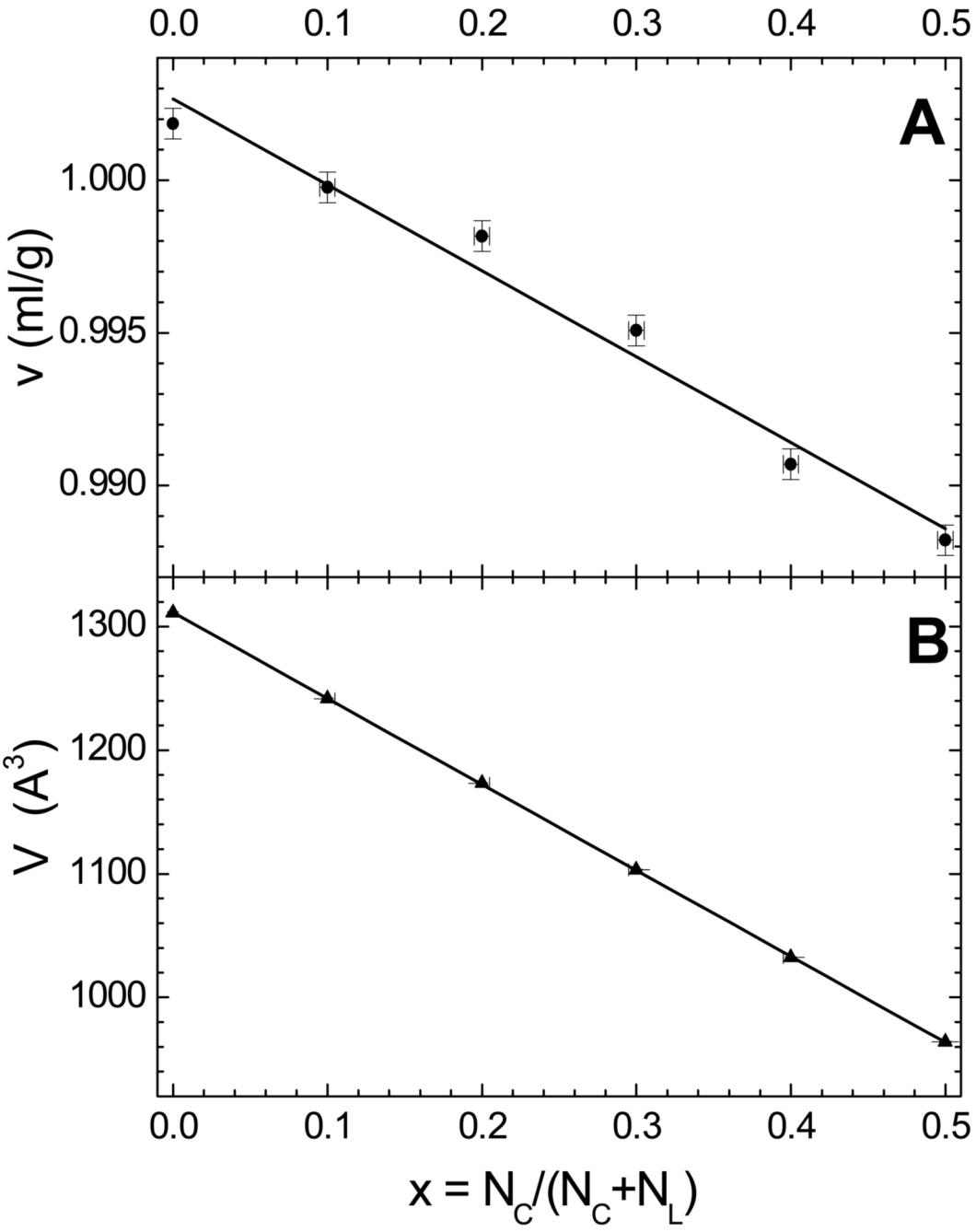

Figure 1.

A. Apparent specific volumes *v* (ml/g) vs. cholesterol mole fraction x for SOPC at 30 °C. B. Volume per molecule *V* in $Å^3$ vs. mole fraction of cholesterol x derived [18] from the measured *v(x)* in A.

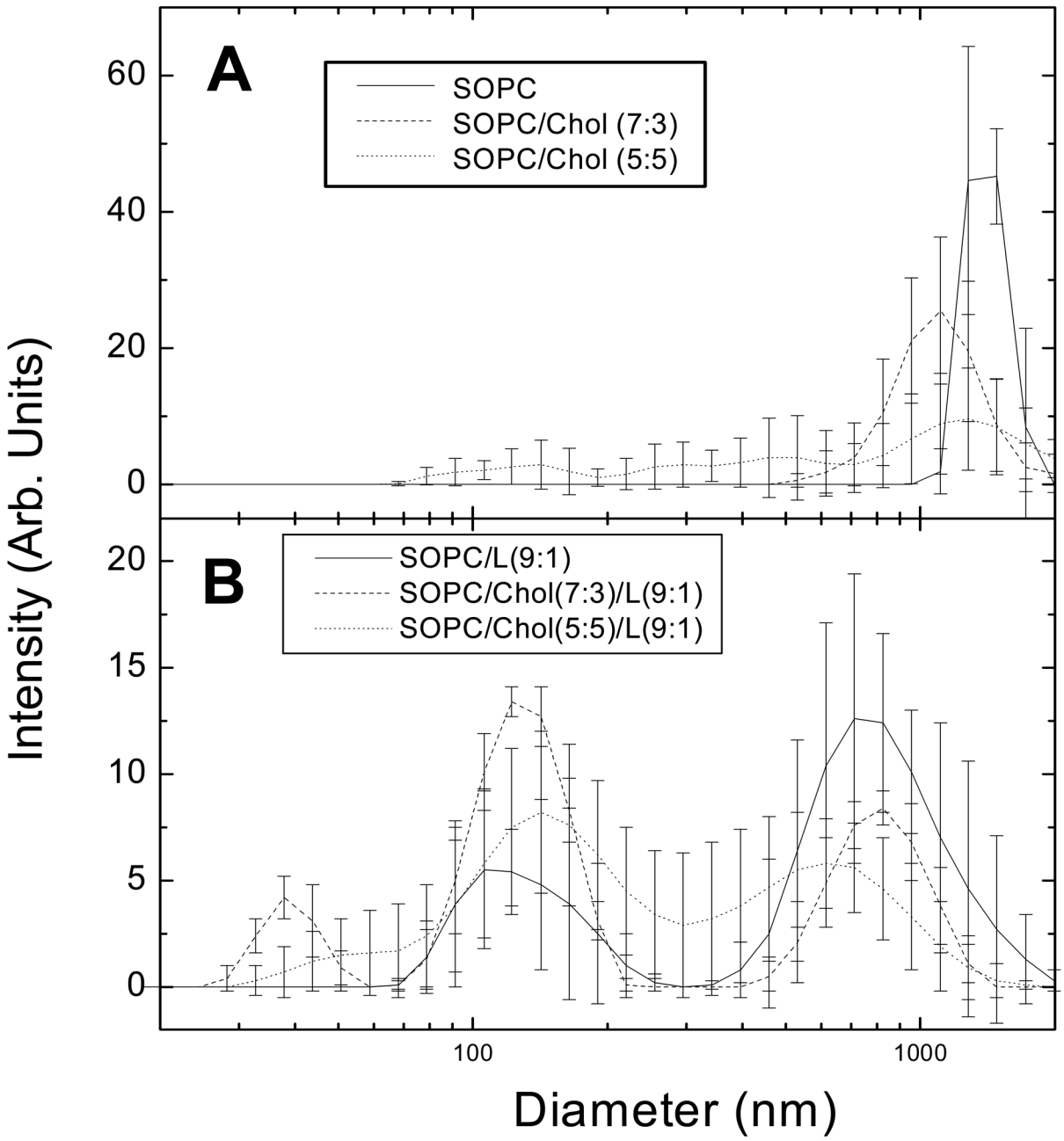

Figure 2.
Particle size results of dynamic light scattering. (A) SOPC with cholesterol (B) SOPC with cholesterol and LWYIK in a 9:1 mole ratio of total lipid to peptide. (Note: SOPC/Chol(7:3)/ L(9:1) can also be described as 0.63:0.27:0.10 SOPC:Chol:LWYIK mole fractions.)

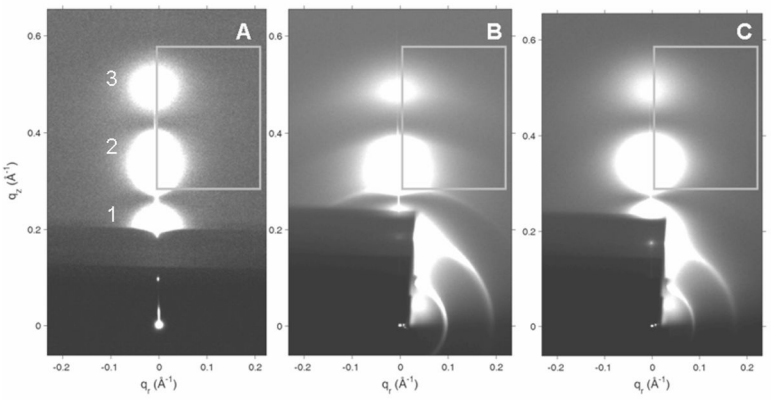

Figure 3.

2D grayscale CCD images of LAXS diffuse scattering data obtained at CHESS at 30 °C. A. SOPC, D-spacing = 63.9 Å, B. SOPC/I (9:1), D-spacing = 67.3 Å, C. SOPC/L (9:1), D-spacing = 81.8 Å. The dark portion for q_z<0.2 Å^{-1} in A and the lower left part of B and C is the shadow cast by the semi-transparent molybdenum beamstop though which the positions of the beam and some of the very intense h=1 and h=2 diffraction peaks can be seen.

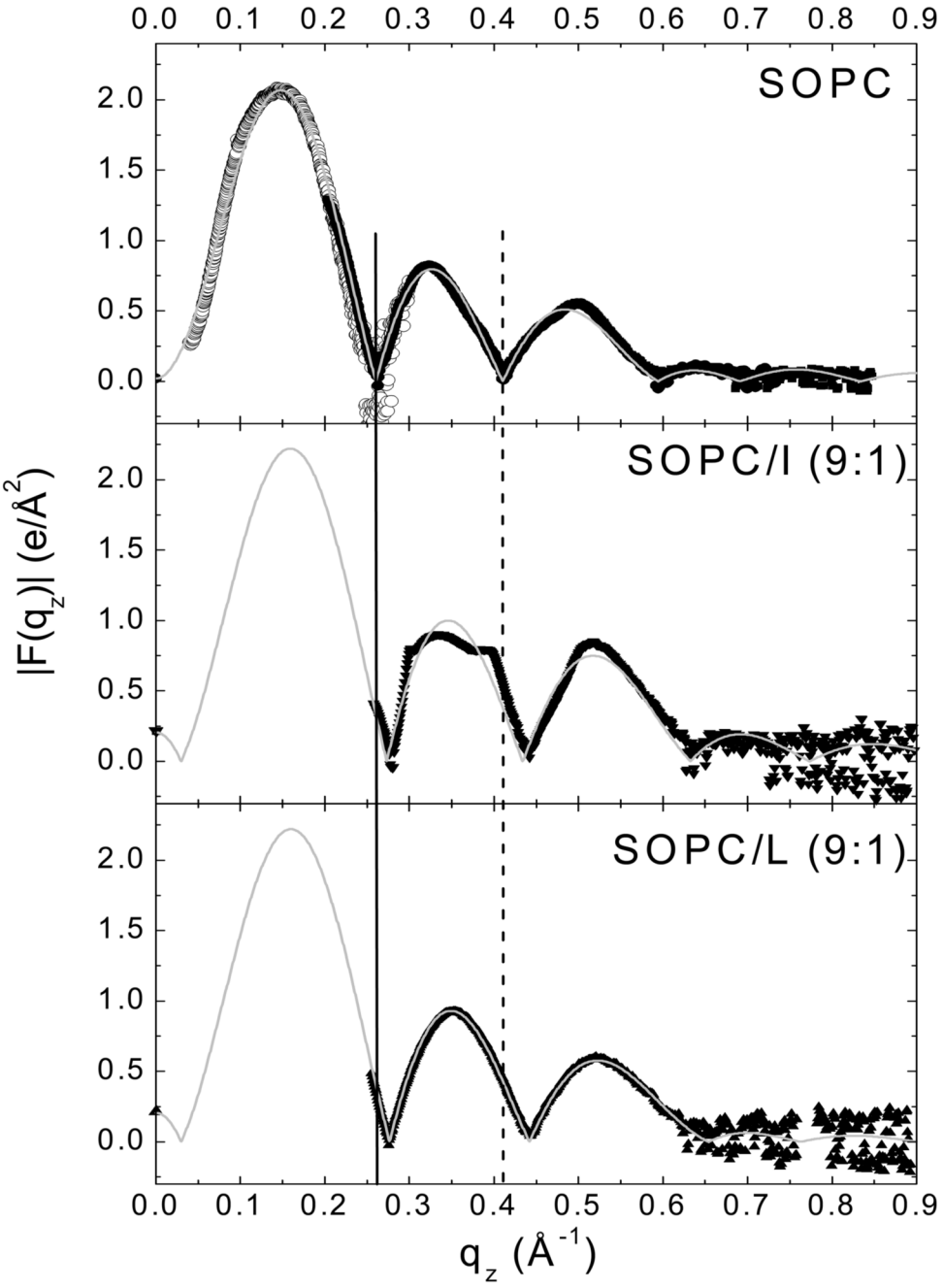

Figure 4.

$|F(q_z)|$ data for SOPC, SOPC/I (9:1) and SOPC/L (9:1). Solid symbols represent data from oriented samples. Open symbols for SOPC only were obtained from unilamellar vesicles (ULV). The solid and dotted vertical lines show shifts in the q values for the zeros in $|F(q_z)|$ compared to SOPC. The thin solid curves show the fits of the H2 model to the data.

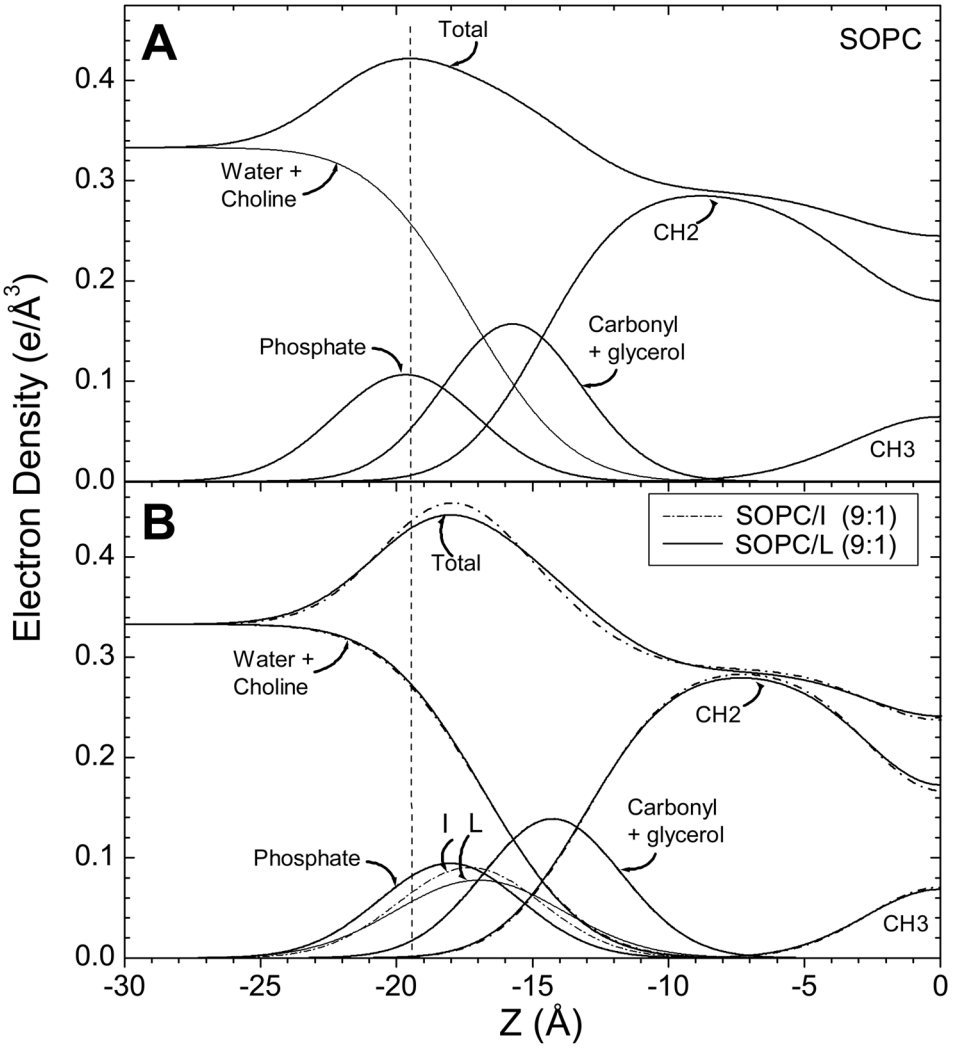

Figure 5.
Electron density profiles of SOPC (A) and SOPC/peptides (B) obtained using the H2 model [17] with a Gaussian added for the peptides. Component groups are labeled and the thinning of the bilayer caused by either peptide is emphasized by the dotted vertical line.

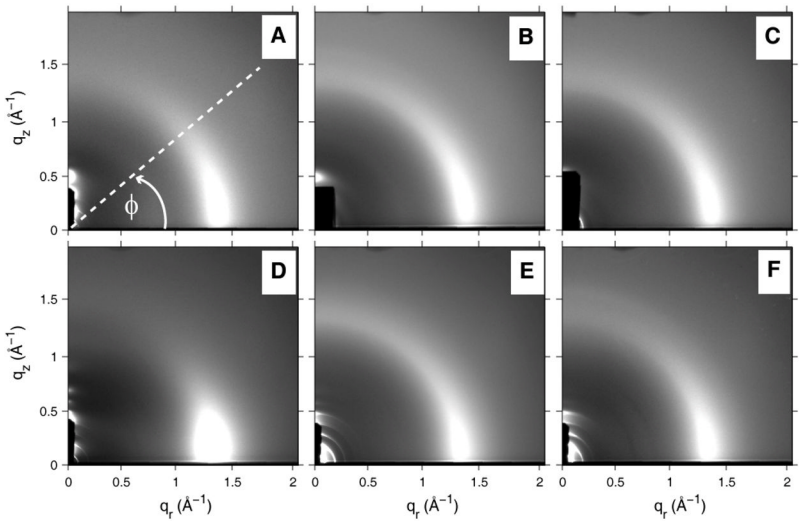

Figure 6.

2D grayscale CCD images of WAXS from oriented samples at 30 °C. (A) SOPC (Φ angle is defined) (B) SOPC/I (9:1) (C) SOPC/L (9:1) (D) SOPC/Chol (7:3) (E) SOPC/Chol (7:3)/I (9:1) (F) SOPC/Chol (7:3)/L (9:1). The LAXS scattering is concentrated along the q_z axis and is partially blocked by the beam stop which is seen on the image as a dark vertical strip near the origin.

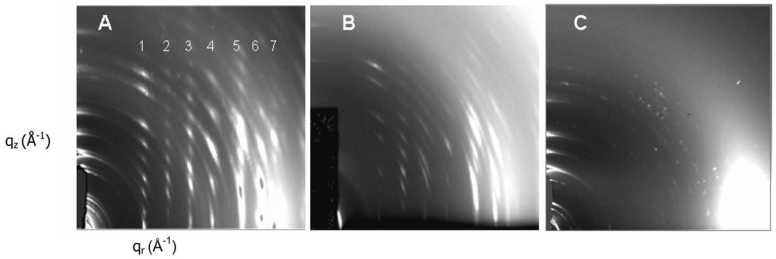

Figure 7.
2D CCD images of crystalline x-ray wide-angle diffraction patterns in the dried state of (A) SOPC/Chol (5:5)/I (9:1) (B) SOPC/Chol (5:5)/L (9:1) (C) SOPC/Chol (5:5).

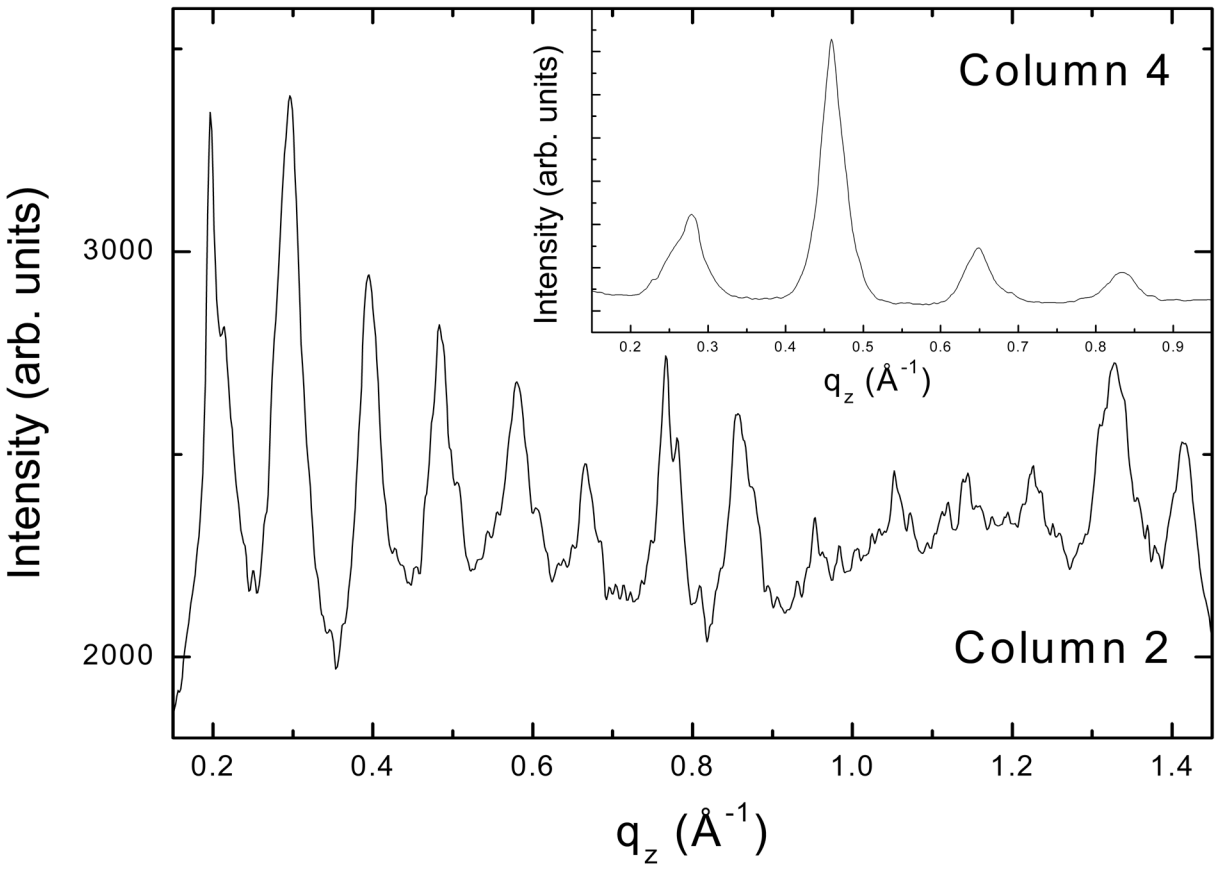

Figure 8.
Vertical slices through q_z in columns 2 and 4 in Fig. 7A, SOPC/Chol(5:5)/I (9:1). D-spacing = 68 ± 2 Å using all the reflections in column 2 and D-spacing = 34.3 ± 0.2 Å using four reflections in column 4.

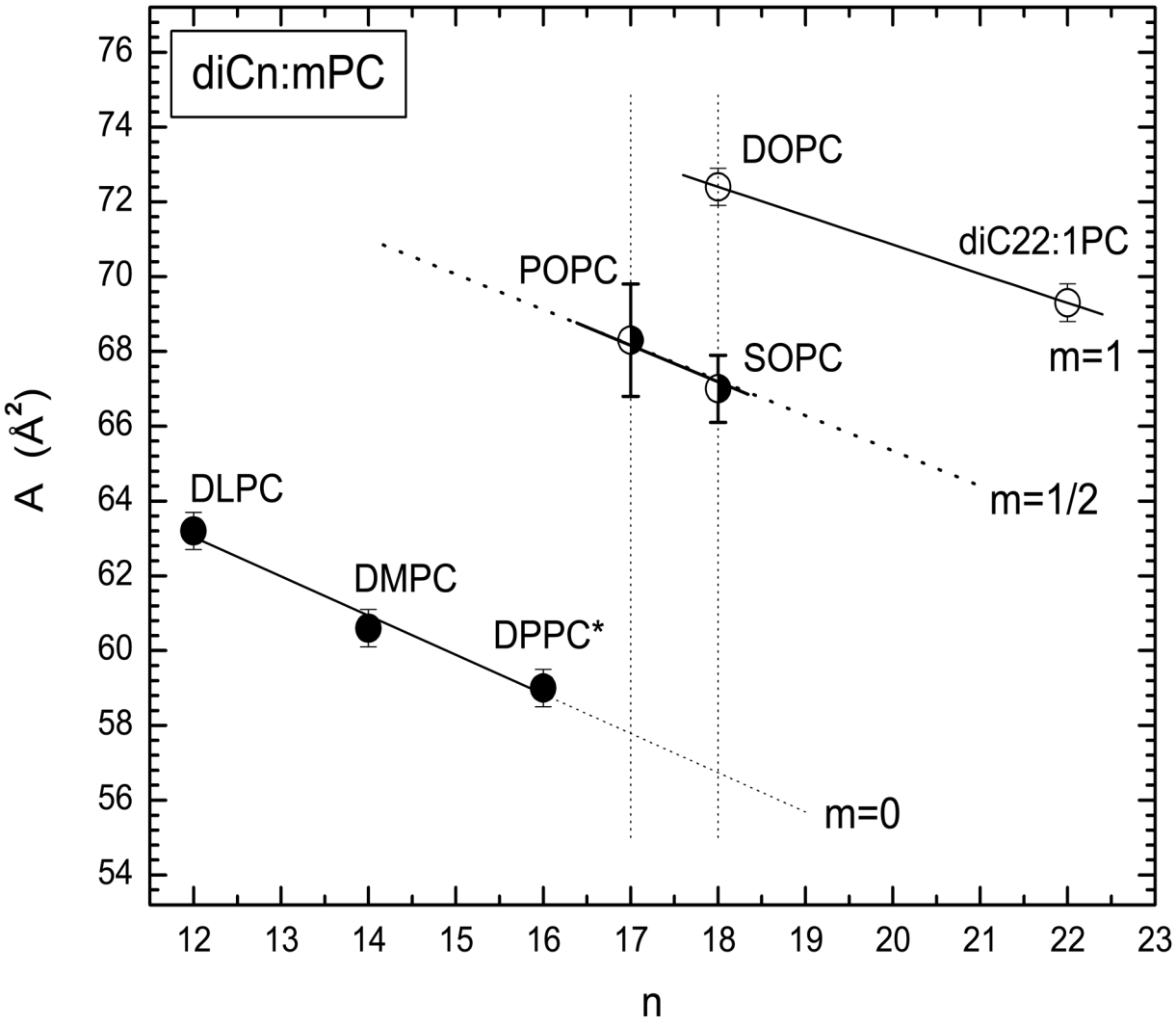

Figure 9.
Summary of areas A_L obtained at T=30 °C for various PCs from diffuse x-ray scattering data using similar methods [9-12], where n=average carbons/lipid and m is the average chain unsaturation, with m=1/2 for each unsaturated chain. *DPPC data were obtained at 50 °C and extrapolated to 30 °C [12].

Table 1

X-ray Spacings

Sample	LAXS, D (Å)	WAXS, d (Å)
SOPC	65.7 ± 0.1	4.52 ± 0.02
SOPC/Chol (7:3)	68.3 ± 0.2	4.75 ± 0.05
SOPC/Chol (5:5)	67.6 ± 0.4	4.89 ± 0.02
SOPC/I (9:1)	Unbound	4.58 ± 0.04
SOPC/Chol (7:3)/I (9:1)	68.9 ± 0.5	4.72 ± 0.06
SOPC/Chol (5:5)/I (9:1)	67.2 ± 0.5	4.75 ± 0.05
SOPC/L (9:1)	Unbound	4.59 ± 0.02
SOPC/Chol (7:3)/L (9:1)	68.8 ± 0.5	4.75 ± 0.05
SOPC/Chol (5:5)/L (9:1)	67.1 ± 0.5	5.01 ± 0.11

LAXS D-spacings were obtained from MLVs in excess water in capillaries, and WAXS d-spacings were obtained from capillary and oriented samples.

Table 2

Structure and Interaction Results

Sample	K_C(x10^{-13}ergs)	D_{HH}	$2D_C$ (Å)	A (Å^2)	$2Z_{pep}$	S_{xray}
SOPC	9.0±1.2	39.0	29.2±0.4	67.0±0.9	--	0.33 ± 0.03
SOPC/I (9:1)	2.3±0.2	36.0	26.1	75.7†	34.6	0.22 ± 0.02
SOPC/L (9:1)	4.2±0.4	36.0	26.2	75.8†	34.0	0.24 ± 0.02
SOPC/Chol (7:3)	13.5±0.5*	42.8*	32.9*	73.8±1.0*†	--	0.65 ± 0.06
SOPC/Chol (7:3)/ I (9:1)	2.4±1.3	41.2	--	--	--	0.39 ± 0.04
SOPC/Chol (7:3)/ L (9:1)	3.8±0.5	41.1	--	--	--	0.37 ± 0.04

*From Ref. 14,

†area/unit cell(lipid+additive)